

Wet etching and passivation of GaSb-based very long wavelength infrared detectors

Xue-Yue Xu(许雪月), Jun-Kai Jiang(蒋俊锴), Wei-Qiang Chen(陈伟强), Su-Ning Cui(崔素宁), Wen-Guang Zhou(周文广), Nong Li(李农), Fa-Ran Chang(常发冉), Guo-Wei Wang(王国伟), Ying-Qiang Xu(徐应强), Dong-Wei Jiang(蒋洞微), Dong-Hai Wu(吴东海), Hong-Yue Hao(郝宏玥), and Zhi-Chuan Niu(牛智川)

Citation: Chin. Phys. B, 2022, 31 (**6**): 068503. DOI: 10.1088/1674-1056/ac4cc1
Journal homepage: http://cpb.iphy.ac.cn; http://iopscience.iop.org/cpb

What follows is a list of articles you may be interested in

Impact of symmetric gate-recess length on the DC and RF characteristics of InP HEMTs

Ruize Feng(封瑞泽), Bo Wang(王博), Shurui Cao(曹书睿), Tong Liu(刘桐), Yongbo Su(苏永波), Wuchang Ding(丁武昌), Peng Ding(丁芃), and Zhi Jin(金智)

Chin. Phys. B, 2022, 31 (**1**): 018505. DOI: 10.1088/1674-1056/ac364d

Improved blue quantum dot light-emitting diodes via chlorine passivated ZnO nanoparticle layer

Xiangwei Qu(瞿祥炜), Jingrui Ma(马精瑞), Siqi Jia(贾思琪), Zhenghui Wu(吴政辉), Pai Liu(刘湃), Kai Wang(王恺), and Xiao-Wei Sun(孙小卫)

Chin. Phys. B, 2021, 30 (**11**): 118503. DOI: 10.1088/1674-1056/ac22a3

Performance analysis of GaN-based high-electron-mobility transistors with postpassivation plasma treatment

Xing-Ye Zhou(周幸叶), Xin Tan(谭鑫), Yuan-Jie Lv(吕元杰), Guo-Dong Gu(顾国栋), Zhi-Rong Zhang(张志荣), Yan-Min Guo(郭艳敏), Zhi-Hong Feng(冯志红), and Shu-Jun Cai(蔡树军)

Chin. Phys. B, 2021, 30 (**2**): 028502. DOI: 10.1088/1674-1056/abb7f6

Performance enhancement of ZnO nanowires/PbS quantum dot depleted bulk heterojunction solar cells with an ultrathin Al_2O_3 interlayer

Shuaipu Zang(臧帅普), Yinglin Wang(王莹琳), Meiying Li(李美莹), Wei Su(苏蔚), Meiqi An(安美琦), Xintong Zhang(张昕彤), Yichun Liu(刘益春)

Chin. Phys. B, 2018, 27 (**1**): 018503. DOI: 10.1088/1674-1056/27/1/018503

Improved performance of Ge n^+/p diode by combining laser annealing and epitaxial Si passivation

Chen Wang(王尘), Yihong Xu(许怡红), Cheng Li(李成), Haijun Lin(林海军)

Chin. Phys. B, 2018, 27 (**1**): 018502. DOI: 10.1088/1674-1056/27/1/018502

RAPID COMMUNICATION

Wet etching and passivation of GaSb-based very long wavelength infrared detectors

Xue-Yue Xu(许雪月)[1,2], Jun-Kai Jiang(蒋俊锴)[1,2], Wei-Qiang Chen(陈伟强)[1,2], Su-Ning Cui(崔素宁)[1,2], Wen-Guang Zhou(周文广)[1,2], Nong Li(李农)[1,2], Fa-Ran Chang(常发冉)[1], Guo-Wei Wang(王国伟)[1,2], Ying-Qiang Xu(徐应强)[1,2], Dong-Wei Jiang(蒋洞微)[1,2], Dong-Hai Wu(吴东海)[1,2], Hong-Yue Hao(郝宏玥)[1,2,†], and Zhi-Chuan Niu(牛智川)[1,2,‡]

[1] *State Key Laboratory for Superlattices and Microstructures, Institute of Semiconductors, Chinese Academy of Sciences, Beijing* 100083, *China*
[2] *College of Materials Science and Opto-Electronic Technology, University of Chinese Academy of Sciences, Beijing* 100049, *China*

(Received 29 November 2021; revised manuscript received 5 January 2022; accepted manuscript online 19 January 2022)

The etching and passivation processes of very long wavelength infrared (VLWIR) detector based on the InAs/GaSb/AlSb type-II superlattice have been studied. By studying the effect of each component in the citric acid solution (citric acid, phosphoric acid, hydrogen peroxide, deionized water), the best solution ratio is obtained. After comparing different passivation materials such as sulfide + SiO_2, Al_2O_3, Si_3N_4 and SU8, it is found that SU8 passivation can reduce the dark current of the device to a greater degree. Combining this wet etching and SU8 passivation, the R_0A of VLWIR detector with a mesa diameter of 500 μm is about 3.6 Ω·cm^2 at 77 K.

Keywords: InAs/GaSb/AlSb superlattice, very long wavelength infrared (VLWIR) detector, wet etching, passivation

PACS: 85.60.Gz, 73.61.Ey, 68.65.Cd **DOI:** 10.1088/1674-1056/ac4cc1

1. Introduction

Antimonide-based type-II superlattice (T2SL) has great potential as infrared materials which is the focus of the world's attention, with outstanding advantages such as adjustable band gap,[1–4] good material uniformity, and large effective mass of electrons.[5] It has important applications in the field of infrared detection, especially in the field of very long wavelength infrared (VLWIR), and it is the material choice for new generation infrared detectors. At present, VLWIR detectors based on antimonide type-II superlattices play an important role in both military and civilian applications.

The dark current is a main parameter to measure the performance of the detector, and in the very long wavelength infrared device, the surface leakage current is the main component of the dark current. During device preparation, the mesa side walls of the etched superlattice material generate suspended and unsaturated bonds, further leading to the generation of surface charges. When the surface energy band is curved, these surface charges accumulate on the sidewall of the mesa or reverse polarity. Then, when a bias voltage is applied to the device, they form a conductive path, which causes surface leakage current.[6,7] Therefore, the etching process effect and passivation process effect in the process of preparing the device play a decisive role in the surface leakage current. Optimizing the etching process and the passivation process can make the performance of the VLWIR detector a big step forward.

In this paper, we first studied the solution selection and ratio of wet etching of the InAs/GaSb/AlSb superlattice VLWIR detector, and then studied the passivation method more suitable for this detector.

The structure of the VLWIR detector used in this paper was grown by the Veeco Gen-II molecular beam epitaxy (MBE) system, with the N-on-P structure, as shown in Fig. 1.

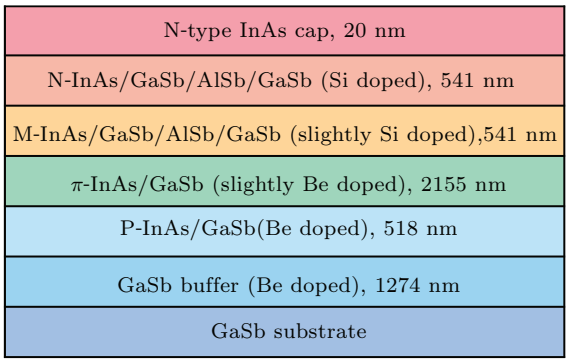


Fig. 1. The structure of VLWIR detector.

In this paper, the electrical performance test was carried out with the Semiconductor Device Parameter Analyzer of Agilent B1500 and the Cryogenic Probe Station of Lakeshore Model CPX. The spectral response was measured by Fourier transform infrared spectrometer of Bruker Vertex 80.

†Corresponding author. E-mail: haohongyue@semi.ac.cn
‡Corresponding author. E-mail: zcniu@semi.ac.cn

© 2022 Chinese Physical Society and IOP Publishing Ltd

2. Etching

The etching process can be roughly classified into wet etching and dry etching. Although the pattern accuracy of dry etching is high, there are a large number of dangling bonds on the sidewall of the device, which will damage the sample surface to a certain extent.[8–10] Therefore, in the preparation of unit devices, wet etching with advantages such as good controllability, clean surface, and low cost is more suitable.

The improper selection of the wet etching solution will make the surface of the device rough, resulting in increased surface leakage current. The selection criterion of the etching solution is that when InAs, AlSb and GaSb are etched, additional chemical products insoluble in acid and alkali will not be generated, and a smooth surface will be obtained. Studies have shown that there are many kinds of acidic solutions that can etch InAs/GaSb. However, InAs, AlSb and GaSb have different physical and chemical properties, and the chemical reactions when they encounter acids are also different. For example, the hydrochloric acid (HCl) solution can etch GaSb, but hardly etch InAs. The citric acid/hydrogen peroxide ($C_6H_8O_7/H_2O_2$) solution is just the opposite, and any volume ratio of this solution will hardly etch GaSb.[11] Therefore, choosing the appropriate etching solution is very important for etching InAs/AlSb/GaSb. In addition, during wet etching, the superlattice material will be easily affected by the etching conditions and the content of each element in the etching solution.

Research has shown that,[12] citric acid-based etching solutions (citric acid, phosphoric acid, hydrogen peroxide and deionized water) can simultaneously react with InAs, AlSb and GaSb, and the reaction rates are similar. In other words, it is the best choice for wet etching. From the chemical mechanism, the superlattice material is first oxidized by hydrogen peroxide and then complexed with phosphoric acid to produce a complex, which is finally dissolved by citric acid.[12–14] The process of the chemical reaction is as follows.[12,15] First, the material is oxidized by hydrogen peroxide (M = Ga, As, Al, Sb or In)

$$4M^{3+} + 6O^{2-} \Leftrightarrow 2M_2O_3. \tag{1}$$

The following reactions will occur in the solution afterwards:

$$2H_2O_2 \Leftrightarrow 2H_2O + O_2, \tag{2}$$

$$H_3PO_4 + 3H_2O \Leftrightarrow PO_4^{3-} + 3H_3O^+, \tag{3}$$

$$2M_2 + 2H_2O_2 + 4H_3PO_4 + 2O_2 + 12H_2O \Leftrightarrow 4M^{3+} + 4PO_4^{3-} + 12H_3O^+ + 6O^{2-} + 2H_2O. \tag{4}$$

In summary, the chemical reaction process can be simplified as

$$2M_2 + 2H_2O_2 + 4H_3PO_4 + 2O_2 + H_2O \Leftrightarrow 2MPO_4 + M_2O_3 + 2PO_4^{3-} + 6H_3O^+. \tag{5}$$

Therefore, we choose to use citric acid-based etching solution, phosphoric acid (85%), hydrogen peroxide (30%), citric acid powder and deionized water mixed in different proportions for wet etching. The full text uses scanning electron microscope (SEM) with the model of NanoSEM 650 and atomic force microscope (AFM) with the model of Dimension Edge to determine the roughness of the sidewall and lower surface of the mesa, and uses the step profiler with the model of KLA-Tencor P7 to measure the corrosion depth and determine the corrosion rate.

First, doing single-variable etching experiments with phosphoric acid, hydrogen peroxide, citric acid and deionized water to analyze the trend of changes brought about by different solute contents. Then combing the chemical reaction mechanism to analyze the experimental phenomenon. The first result of the single variable experiment shows that as the content of hydrogen peroxide increases, the corrosion rate increases, and the sidewall and lower surface of the mesa gradually become smoother. Then, when the content of hydrogen peroxide gradually increases to a certain extent, the corrosion rate will only increase slightly, and the side walls and lower surface of the mesa begin to gradually become rough, as shown in Table 1. Secondly, the increase of phosphoric acid will greatly increase the corrosion rate, as shown in Table 2.

Table 1. Etching rate and roughness of different volumes of H_2O_2.

	H_2O_2 (ml)	Etching rate ($nm \cdot min^{-1}$)	Surface roughness (nm)
1	3	48	4.56
2	18	133	1.81
3	30	207	5.24
4	42	242	Grey
5	66	251	Grey

Table 2. Etching rate of different volumes of H_3PO_4.

	H_3PO_4 (ml)	Etching rate ($nm \cdot min^{-1}$)
1	6	27
2	30	133
3	54	234

Thirdly, with the increase of citric acid content, the corrosion rate increases and the sidewall morphology becomes smooth. Excessive increase will cause the sidewall gully to increase slightly, but will not make the sidewall too rough, as shown in Table 3. Finally, with the increase of deionized water content, the corrosion rate decreases, as shown in Table 4.

Table 3. Etching rate and roughness of different volumes of $C_6H_8O_7$.

	$C_6H_8O_7$ (g)	Etching rate ($nm \cdot min^{-1}$)	Surface roughness (nm)
1	3	88	Grey
2	10.5	129	4.32
3	15	133	1.81
4	33	147	2.76

Table 4. Etching rate of different volumes of H_2O.

	H_2O (ml)	Etching rate (nm·min^{-1})
1	600	133
2	750	112
3	900	62

Combined with the chemical reaction mechanism, the above experimental results can be reasonably explained. In the first step, the hydrogen peroxide reacts with the material to produce oxide (M_2O_3). Firstly, when the content of hydrogen peroxide is insufficient, the oxides generated by the oxidation reaction will also be insufficient. However, the content of phosphoric acid is relatively excessive at this time, which will directly corrode the material and make the surface morphology of the material rough. Then, when the content of hydrogen peroxide is just right, phosphoric acid only reacts with oxide and no longer directly corrodes the material, so the surface morphology of the material is smooth at this time. Finally, when the amount of hydrogen peroxide is excessive, too much oxide is generated, which is not completely reacted by phosphoric acid, causing the surface of the material to become rough again. In the second step, phosphoric acid reacts with oxides to produce complex MPO_4 ($InPO_4$, $GaPO_4$, $AsPO_4$, $AlPO_4$ and $SbPO_4$). Therefore, increasing the amount of phosphoric acid can directly increase the corrosion rate of the solution. In the last step, citric acid plays a role to dissolve these complexes attached to the surface of the material. When the content of citric acid is insufficient, the resulting complex is not completely reacted, causing the surface of the material to become rough. And when the content of citric acid is just right, the morphology of the side wall and lower surface of the mesa becomes smooth. Then, when the content of citric acid is excessive, the excess citric acid will directly corrode InAs and AlSb. However, the citric acid is not as strong as the phosphoric acid, so it only causes a slight increase in the gullies on the side wall. In addition, the appropriate increase of various solutes will accelerate the chemical reactions and increase the corrosion rate. But, when the solute is increased in excess, the chemical reactions in which it is not involved drag down the overall process and the amplitude of increase in corrosion rate is reduced.

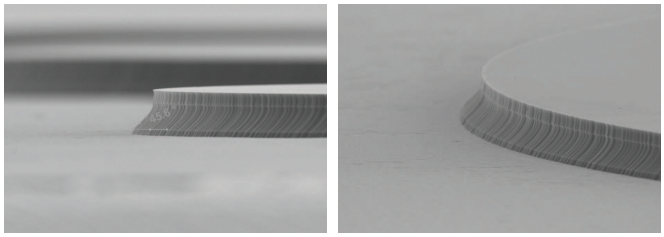


Fig. 2. The SEM image of the device sidewall corrosion interface. The ratio of corrosive solution is $C_6H_8O_7$:H_3PO_4:H_2O_2:H_2O = 0.45 g:1 ml:0.6 ml:20 ml.

After many experiments, it is finally determined that the solution ratio is $C_6H_8O_7$:H_3PO_4:H_2O_2:H_2O = 0.45g:1 ml:0.6 ml:20 ml. From the SEM image (Fig. 2), it can be seen that the mesa etched by the citric acid solution with this ratio has the advantage of high line accuracy. The inclination angle of the sidewall is about 45°, and the morphology is smooth without attached particle contamination. Besides, surface roughness is 0.24 nm, as shown in Fig. 3, and Fig. 4 shows the dark current and *RA* curves of devices with different mesa sizes. The results show that the device has good performance, and with the increase of mesa diameter, the dark current density decreases and the device performance improves.

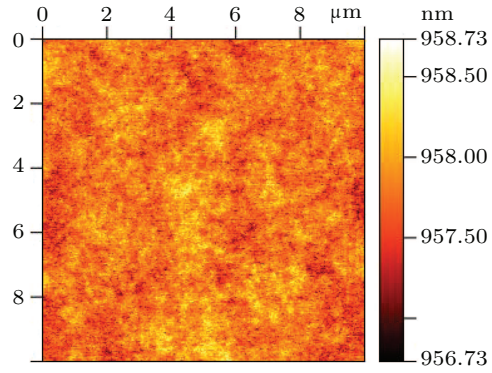


Fig. 3. AFM image of the surface. The ratio of corrosive solution is $C_6H_8O_7$:H_3PO_4: H_2O_2:H_2O=0.45g:1 ml:0.6 ml:20 ml.

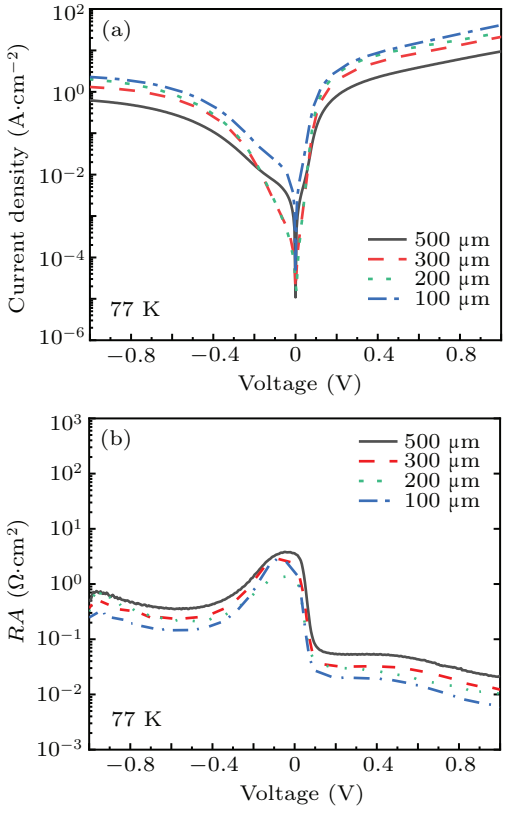


Fig. 4. Characterization of electrical properties of different mesa sizes at 77 K: (a) dark current density, (b) *RA*.

The device with a mesa diameter of 500 μm reaches saturation at a forward bias of 150 mV, and the 100% cut-off wavelength is about 19.06 μm, as shown in Fig. 5.

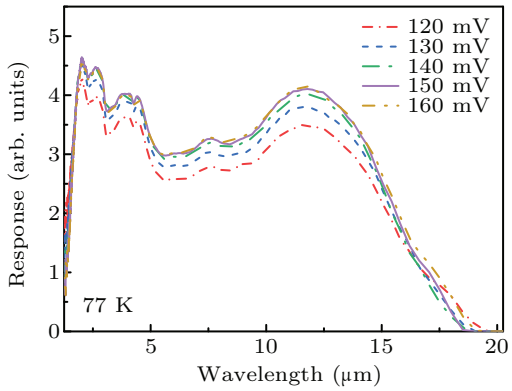


Fig. 5. Spectral response of VLW infrared detector.

Experiments have proved that the movement state of the sample during wet etching will also affect the corrosion rate when the solution ratio is determined. Besides, if the sample is in a static state during wet etching, the corrosion rate will gradually decrease with the increase of the corrosion time. The corrosion depth of this sample is approximately 3700 nm. When the sample is in a static state during wet etching, the corrosion rate of the corrosion solution at this ratio is about 140 nm/min. When the sample keeps moving during wet etching, the corrosion rate is about 200 nm/min.

3. Passivation

Since the etching process destroys the periodic structure of the crystal, a large number of unsaturated bonds and dangling bonds are generated on the surface of the device. If they are not treated by the passivation process, they will adhere to impurities or be oxidized during later processes to form surface potential,[16] and this can cause the surface energy band to bend, resulting in surface leakage current.[6,7] Therefore, the passivation process plays an important role in the preparation of high-performance infrared detectors.

At present, the passivation methods include chemical passivation (such as ammonium sulfide[17]), dielectric layer deposition (such as Si_xN_y,[18] SiO_2,[19,20] Al_2O_3[21]), polyimide passivation,[22] and so on.

In order to suppress surface leakage, this paper compares and studies the most suitable passivation methods for the InAs/GaSb/AlSb superlattice VLWIR detector, including sulfide + SiO_2, Al_2O_3, Si_3N_4 and SU8 passivation.

The sulfide solution is made up of sodium sulfide nonahydrate and ethylene glycol. First, anodic sulfidation was performed, followed by the growth of 200 nm SiO_2 using PECVD. Al_2O_3, with a thickness of 30 nm, was grown by ion beam sputtering with high growth quality and good adhesion. Si_3N_4, with a thickness of 200 nm, was grown by PECVD. The photoresist of SU8 2000 series is suitable for the sidewall of almost vertical slope. Specifically, SU8 2010 is selected for passivation. when the glue homogenizer is 4000 rpm, the glue thickness is about 9.5 μm. The dark current and *RA* curve of the device with a mesa diameter of 500 μm are shown in Fig. 6.

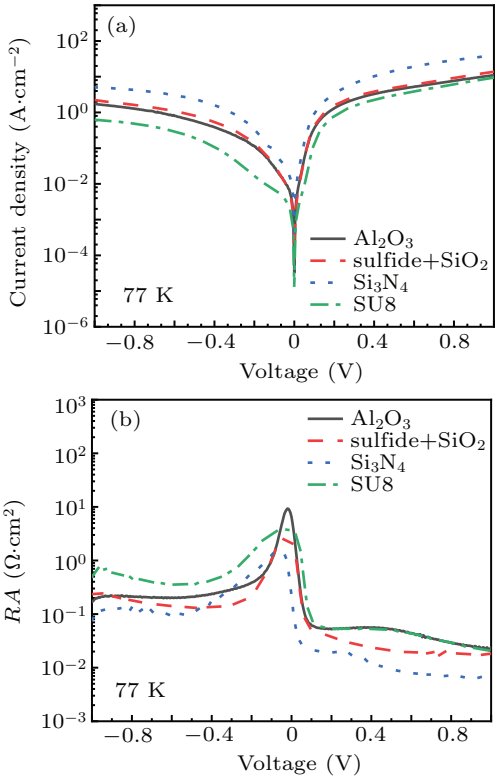


Fig. 6. Characterization of electrical properties of different passivation methods at 77 K: (a) dark current density, (b) *RA*.

For the InAs/GaSb/AlSb superlattice VLWIR detector, the device using the SU8 2010 passivation process has the best performance, and when the temperature is 77 K, the R_0A of the device with a mesa diameter of 500 μm is about 3.6 Ω·cm^2. The effects of sulfide +SiO_2 passivation and Al_2O_3 passivation are tied for the second place. The passivation effect of Si_3N_4 is the worst of the four.

Combined with chemical mechanism and process method, the effect of the above passivation process can be explained. After SU8 is hard baked, the physical and chemical properties are stable, and the dark current of the device is reduced. Vulcanization is a kind of chemical passivation, which can saturate the suspension bond with sulfur and eliminate the sidewall suspension bond. Growing SiO_2 film for physical passivation, which can prevent the material from contacting with the external environment and prolong the lifespan. Al_2O_3 has a relatively small fixed charge density, and the sidewall energy band will hardly reverse or accumulate. There are many intrinsic charges in Si_3N_4, which is easy to form charge conduction channels along the sidewall and reduce the performance of the device.

4. Conclusion

To sum up, in the VLWIR detector, low dark current is one of the necessary conditions for the detector to reach the high-performance standard. The surface leakage current, as

the main component of the dark current in the VLWIR detector, is largely affected by the etching and passivation process. Therefore, optimizing the device preparation process is a key step. First, a citric acid solution is used for wet etching. By studying the effect of each component in the etching solution, it is optimized that when the ratio of corrosion solution is $C_6H_8O_7$:H_3PO_4:H_2O_2:H_2O = 0.45 g:1 ml:0.6 ml:20 ml, the surface of the etched device can be smooth without precipitates. For the passivation process, the passivation effects of sulfide + SiO_2, Al_2O_3, Si_3N_4, and SU8 are compared. According to the experiments, it is concluded that SU8 passivation can optimize the device performance to a greater degree and reduce the dark current. Combining this wet etching and SU8 passivation, when the temperature is 77 K, the R_0A of the device with a mesa diameter of 500 μm is about 3.6 Ω·cm^2.

Acknowledgements

Project supported by the National Basic Research Program of China (Grant Nos. 2018YFA0209102 and 2019YFA070104), the National Natural Science Foundation of China (Grant Nos. 61790581 and 61274013), the Key Research Program of the Chinese Academy of Sciences (Grant No. XDPB22).

References

[1] Walther M, Schmitz J, Rehm R, *et al*. 2005 *J. Cryst. Growth* **278** 156
[2] Wei Y, Hood A, Yau H, *et al*. 2005 *Appl. Phys. Lett.* **86** 4785
[3] Sullivan G J, Ikhlassi A, Bergman J, *et al*. 2005 *J. Vac. Sci. Technol. B* **23** 1144
[4] Aifer E H, Jackson E M, Boishin G, *et al*. 2003 *Appl. Phys. Lett.* **82** 4411
[5] Smith D L and Mailhiot C 1987 *J. Appl. Phys.* **62** 2545
[6] Chen G, Nguyen B M, Hoang A M, *et al*. 2011 *Appl. Phys. Lett.* **99** 651
[7] Chen G, Huang E K, Hoang A M, *et al*. 2012 *Appl. Phys. Lett.* **101** 651
[8] Delaunay P Y, Nguyen B M, Hoffman D, *et al.* 2009 *IEEE Journal of Quantum Electronics* **45** 157
[9] Huang E K, Nguyen B M, Hoffman D, *et al*. 2009 *Proc. SPIE* **7222** 72220
[10] Huang E K, Hoffman D, Nguyen B, *et al*. 2009 *Appl. Phys. Lett.* **94** 163511
[11] Plis E A, Kutty M N and Krishna S 2013 *Laser & Photon. Rev.* **7** 45
[12] Chaghi R, Cervera C, Grech P, *et al*. 2009 *Semiconductor Science and Technology* **24** 065010
[13] Dier O, Lin C, Grau M, *et al*. 2004 *Semiconductor Science and Technology* **19** 1250
[14] Kutty M N, Plis E, Khoshakhlagh A, *et al*. 2010 *J. Electron. Mater.* **39** 2203
[15] Hao H Y, Xiang W, Wang G W, *et al.* 2015 *Chin. Phys. Lett.* **32** 107302
[16] Plis E A 2014 *Advances in Electronics* **2014** 1
[17] Lebedev M V, Lvova T V, Pavlov S I, *et al*. 2017 *Semiconductors* **51** 1093
[18] Ying Z, Ji X, Ming S, *et al*. 2015 *Journal of Applied Physics* **118** 034507
[19] Hood A, Razeghi M, Aifer E H, *et al*. 2005 *Appl. Phys. Lett.* **87** 3262
[20] Plis E A, Kutty M N and Krishna S 2013 *Laser & Photon. Rev.* **7** 45
[21] Huang M L, Chang Y C, Chang C H, *et al*. 2005 *Appl. Phys. Lett.* **87** 87
[22] Hood A, Delaunay P Y, Hoffman D, *et al*. 2007 *Appl. Phys. Lett.* **90** 233513